Macrophages undergo a behavioural switch during wound healing in zebrafish

Tamara Sipka, Seol Ah Park, Resul Ozbilgic, Laurence Balas, Thierry Durand, Karol Mikula, Georges Lutfalla, Mai Nguyen-Chi

Free Radical Biology and Medicine 192 (2022) 200–212

Contents lists available at ScienceDirect

Free Radical Biology and Medicine

journal homepage: www.elsevier.com/locate/freeradbiomed

Macrophages undergo a behavioural switch during wound healing in zebrafish

Tamara Sipka [a], Seol Ah Park [b,1], Resul Ozbilgic [a,1], Laurence Balas [c], Thierry Durand [c], Karol Mikula [b], Georges Lutfalla [a], Mai Nguyen-Chi [a,*]

[a] LPHI, Univ Montpellier, CNRS, Montpellier, France
[b] Department of Mathematics and Descriptive Geometry, Slovak University of Technology in Bratislava, Slovakia
[c] IBMM, UMR5247, CNRS, Univ Montpellier, ENSCM, Montpellier, France

ARTICLE INFO

Keywords:
Macrophage
Trafficking
Specialized pro-resolving mediators
Protectin D1
Zebrafish

ABSTRACT

In response to wound signals, macrophages are immediately recruited to the injury where they acquire distinct phenotypes and functions, playing crucial roles both in host defense and healing process. Although macrophage phenotypes have been intensively studied during wound healing, mostly using markers and expression profiles, the impact of the wound environment on macrophage shape and behaviour, and the underlying mechanisms deserve more in-depth investigation. Here, we sought to characterize the dynamics of macrophage recruitment and behaviour during aseptic wounding of the caudal fin fold of the zebrafish larva. Using a photo-conversion approach, we demonstrated that macrophages are recruited to the wounded fin fold as a single wave where they switch their phenotype. Intravital imaging of macrophage shape and trajectories revealed that wound-macrophages display a highly stereotypical set of behaviours and change their shape from amoeboid to elongated shape as wound healing proceeds. Using a pharmacological inhibitor of 15-lipoxygenase and protectin D1, a specialized pro-resolving lipid, we investigated the role of polyunsaturated fatty acid metabolism in macrophage behaviour. While inhibition of 15-lipoxygenase using PD146176 or Nordihydroguaiaretic acid (NDGA) decreases the switch from amoeboid to elongated shape, protectin D1 accelerates macrophage reverse migration and favours elongated morphologies. Altogether, our findings suggest that individual macrophages at the wound switch their phenotype leading to important changes in behaviour and shape to adapt to changing environment, and highlight the crucial role of lipid metabolism in the control of macrophage behaviour plasticity during inflammation *in vivo*.

1. Introduction

Healing a wound is an essential process to maintain body integrity and protect from pathogens. Therefore, animals have evolved an efficient response to restore barrier integrity and repair tissue damages based on a self-limited inflammation [1]. Macrophages are amid the first cells to be recruited to the injury site where they play instrumental roles in orchestrating the different steps of the healing process, from host defense to repair [2]. Depletion of macrophages in animal models results in impaired wound healing [3–5] and impaired regeneration in mammals [6–8] and non-mammalian species [9–13]. Therefore, therapeutic strategies targeting macrophage function may represent valuable tools to orchestrate healing process during trauma or chronic wounds.

Macrophages display a high-functional plasticity with respect to shape, behaviour and gene expression program. After exposure to specific signals from the microenvironment, they adopt distinct functional phenotypes by a process called polarization. Traditionally, macrophages are thought to be recruited at the wound in two phases [2]. Macrophages first polarize towards a pro-inflammatory phenotype, and express pro-inflammatory cytokines, like Tumor Necrosis Factor (TNF) and Interleukin-6 (IL-6) and participate in host defense and debris removal at the wound; they are referred to as M1-like macrophages [14]. Secondly, M2-like macrophages producing Transforming Growth Factor-β1 (TGF- β1) participate in the resolution of inflammation and later wound reparative functions like re-epithelialization and the remodeling of the tissue [5,14]. *In vivo*, microenvironment signals encountered by

* Corresponding author.
E-mail address: mai-eva.nguyen-chi@umontpellier.fr (M. Nguyen-Chi).
[1] These authors contributed equally to this work.

https://doi.org/10.1016/j.freeradbiomed.2022.09.021
Received 20 May 2022; Received in revised form 8 September 2022; Accepted 19 September 2022
Available online 24 September 2022

macrophages are diverse, and, temporally and spatially dynamic. For this reason, macrophages not only respond with equally diverse phenotypes, going beyond M1/M2 phenotypes, but also can switch from one functional phenotype to another [15,16]. The wound-macrophages do probably not derogate from this rule, although the full spectrum of macrophage states at the wound has not been completely explored.

Temporal control of macrophage phenotype from M1-like to M2-like during the resolution process has been shown to be critical in normal wound healing and perturbing this sequence delays healing and regeneration in animal models [5,11,12,17]. However, the mechanistic of macrophage behaviour at the wound still remains unclear. One possibility is that different populations of macrophages are recruited sequentially, in waves; at a specific time point during the healing process, the initial pro-inflammatory population is replaced by the pro-healing population. An alternative scenario would be that macrophages are recruited to the wound in the single wave and that pro-inflammatory macrophages switch their phenotype into anti-inflammatory/reparative macrophages at the injury site during wound healing.

While wound macrophages undergo sequential polarization status, involving deep changes in gene-expression program and function, the changes of macrophage behaviour and shape in response to the local wound milieu are less studied. Using *in vitro* 2-D systems, several studies highlighted a relationship between the morphology of macrophages and their polarization status. However, attributing a shape to a polarization status is tendentious. Polarization assays using murine peritoneal macrophages cultured *in vitro* showed that M1 macrophages displayed an expanded morphology with elongated filopodia and numerous lamellar processes, while M2 macrophages had a morphology similar to that of unstimulated macrophages [18]. Another study reported that M1 macrophages polarized *in vitro* from bone marrow-derived macrophages displayed a round morphology with multiple lamellipodia, while M2 macrophages were more stretched [19]. Rey-Giraud et al. demonstrated that monocyte-derived macrophages have a unique morphology which not only depends on cytokine stimulation but also on culture media [20]. Several studies also point out the influence of surface or milieu properties on human macrophage morphology and behaviour [21,22]. An interesting study further demonstrated that altering the morphology of monocyte-derived macrophages can trigger alterations in the activation status of these cells, suggesting that extracellular matrix architecture provides integral cues to control macrophage polarization [23]. How wound macrophages behave at the site of injury? What are the morphologic and behavioural changes induced in response to the local wound milieu? These questions have not been fully investigated. To date, the molecular mechanisms controlling these changes are unknown.

Recently, specialized pro-resolving mediators (SPM), a group of structurally and chemically distinct polyhydroxylated polyunsaturated fatty acid (PUFA) derivatives including lipoxins, E and D-series resolvins (RvD), protectins and maresins, play critical roles in the resolution of inflammation and decrease disease severity (for review [24–26]). Interestingly several studies report the role of SPM in the control of macrophage function like phagocytosis, cytokine production or polarization [27–30]. Whether SPMs also regulate macrophage shape and motility remains unknown.

Like mammals, the zebrafish possess an innate immune system including macrophages recapitulating anti-microbial defense and pro-inflammatory functions [31] but also reparative and regenerative functions [11–13,32]. Further, the transcriptomic profile of larval zebrafish macrophages revealed high similarities in terms of gene expression with human macrophages [33]. While zebrafish macrophages can migrate toward an injury or an infection site [34], they also show polarization properties upon a threat [11,35,36]. Therefore, the zebrafish larva offers unrivalled opportunities to study, in real time and in 3D tissues, the dynamic behaviour and shape of macrophages during healing.

In the current study we used the zebrafish fin fold injury model and high-resolution imaging of transgenic reporter lines to delineate macrophage behaviour with respect to shape, migration and motility in the changing wound milieu. In particular, we demonstrate that macrophages are recruited in a single wave to the wound where they undergo a behavioural switch between 9 and 11 h post amputation correlating with drastic changes in morphology. These changes are dependent on polyunsaturated fatty acid metabolism. We provide key data to understand macrophage dynamic plasticity during wound healing.

2. Material and methods

2.1. Ethics statement

Animal experimentation procedures were carried out by following the 3Rs - Replacement, Reduction and Refinement principles according to the European Union guidelines for handling of laboratory animals (http://ec.europa.eu/environment/chemicals/lab_animals/home_en.htm) and were approved by the Comité d'Ethique pour l'Expérimentation Animale under reference CEEA-LR- B34-172-37 and APAFIS#5737–2016061511212601 v3.

2.2. Fish husbandry

Zebrafish (*Danio rerio*) maintenance, staging and husbandry were performed at the fish facility of the University of Montpellier as described previously [37]. Wild Type (WT) from AB background were used. Following transgenic lines were used: *Tg(mfap4:mCherry-F) ump6Tg* referred as *Tg(mfap4:mCherry-F)* [38]. *Tg(mpx:eGFP)i114*, referred as *Tg(mpx:GFP)* was used to visualize neutrophils [39]. *Tg (mpeg1:Gal4)GL25* [34] and *Tg(UAS:Kaede)rk8* [40] were used to visualize macrophages and track them by photoconversion. Embryos were obtained from pairs of adult fishes by natural spawning and raised at 28.5 °C in embryo water. Embryos and larvae were staged according to Ref. [41] and used from 3 to 6 days post-fertilization (dpf).

2.2.1. Larva manipulation for wounding and regeneration quantification

The caudal fin fold transection was performed at the larval stage 3 dpf. Larvae were anesthetized with 160 μg/mL buffered tricaine solution (0.016%). The amputation was performed with scalpel, at the limit of notochord posterior end. After the amputation, larvae were placed in tricaine-free zebrafish water containing or not the chemicals, and incubated at 28.5 °C until imaging. Regenerative fin fold length was calculated as the distance between the amputation plane and the edge of the fin fold in the medial plane. Regenerative fin fold area was calculated as the area of the fin fold from the amputation plane and the edge of the fin fold.

2.2.2. Drug treatments of zebrafish larvae

PD146176 (Sigma-Aldrich, P4620) stock was prepared in DMSO at 20 mM. An intermediate stock solution was prepared in DMSO at 500 μM. Larvae were treated with 1.5 μM PD146176 (or same volume of DMSO) added in the fish medium, immediately after the fin fold amputation until the end of experiment.

NDGA (Calbiochem, CAS 500-38-9) stock was prepared in DMSO at 50 mM. An intermediate stock solution was prepared in DMSO at 10 mM. Larvae were treated with 50 μM NDGA (or same volume of DMSO) added in the fish medium, immediately after the fin fold amputation until the end of experiment.

2.2.3. Injections of protectin D1 and resolvin D1 in zebrafish larvae

Protectin (PD1) was synthesized as described [42,43], and dissolved in ethanol as a stock solution at 1 mg/ml. Resolving D1 (RvD1) (Cayman Chemical, 10012554) was dissolved in ethanol as a stock solution at 0.1 mg/ml. Larvae were anesthetized with 0.016% buffered tricaine solution added in the fish water and injected in the posterior caudal vein at 3 dpf with different doses: 100 pg, 200 pg, 400 pg for PD1 and 100 pg, 200

pg, 400 pg, 450 pg for RvD1 or same volume of ethanol (maximum 6 nl of 50% ethanol solution-50% water) as a control, 1 h before the fin fold amputation.

2.2.4. Live imaging of zebrafish larvae

Larvae were anesthetized with 0.016% buffered tricaine, mounted in 1% low melting point agarose in lateral orientation as previously described [44]. Epi-fluorescence microscopy was performed using a MVX10 Olympus microscope (MVPLAPO 1X objective; XC50 camera). Confocal microscopy was performed on ANDOR CSU-W1 confocal spinning disk on an inverted NIKON microscope (Ti Eclipse) with ANDOR Neo sCMOS camera (20x air/NA 0.75 objective); lasers 488 nm (GFP) and 561 nm (mCherry); or ZEISS LSM880 FastAiryscan in a confocal mode, 20 × /NA 0.8 Plane apochromat, the wavelength 561 nm (DSSP Laser) for excitation and 585–620 nm for emission (GaAsP detector). Image stacks for time-lapse movies were acquired at 28 °C with setup described in the legends. The 4D files generated from time-lapse acquisitions were processed using Image J. Brightness and contrast were adjusted for maximal visibility.

2.2.5. Macrophage and neutrophil quantification

ImageJ (Fiji) was used for all manual image analyses and our own algorithm implemented in C language was used for automatic segmentation and tracking of macrophages when studying their dynamics at all time points of time lapse videos. Recruited macrophages and neutrophils were quantified manually from maximum projection images, after brightness and contrast adjustment for better visualization using ImageJ (Fiji). Leukocytes were quantified in the stump region that extends until 270 μm from the edge of the wound. Global macrophage population was quantified by computation using ImageJ (Fiji), as follows: 1/macrophages were detected using "Find Maxima" function, 2/Maxima were automatically counted using run("ROI Manager … "), roiManager ("Add") and 3/roiManager("Measure") functions.

2.2.6. Macrophage tracking and shape analysis

For manual image analysis, macrophages were tracked in every time step using Manual Tracking ImageJ PlugIn. Velocity was extracted directly from manual tracking data table. Directionality graphs were obtained by Chemotaxis and Migration Tool PlugIn using the X–Y position of each macrophage extracted from manual tracking data table. Macrophage wound distance was measured manually, as a shortest distance from the macrophage center to the wound margin. Macrophage perimeter, area and circularity (4π*area/perimeter^2) values were extracted automatically from ImageJ measurements, after the following steps: 1/maximum projection of the image was transformed into binary format, threshold was set using triangle algorithm; 2/isolated macrophages were outlined semi-automatically using wand (tracing) tool, while macrophages overlapping with others were outlined manually with freehand selection tool, when possible. Macrophage shape was quantified in the stump region that extends until 270 μm from the edge of the wound.

For automated image analysis, the image segmentation was carried out from 8 to 13 hpA. At first, the images were filtered by using space-time filtering that keeps the temporal coherence of moving macrophages [45]. Then, the filtered images were segmented by a combination of the local Otsu method [46,47] and (Park et al., unpublished) and the subjective surface segmentation (SUBSURF) method [48] where the binarized images from the local Otsu method were considered as an initial condition of the SUBSURF equation (Park et al., unpublished). Trajectories of macrophages in segmented images were reconstructed based on automatic cell tracking (Park et al., unpublished), and shape descriptors (perimeter and circularity) were measured.

2.2.7. Macrophage tracking by photoconversion

For macrophage tracking, *Tg(mpeg1:gal4/UAS: Kaede)* embryos raised to 3 dpf in the dark. At 8 hpA, larvae were mounted in 1% low-melting agarose and Kaede photoconversion was performed using a 405 nm Laser on a confocal Leica SPE upright microscope (20x CHX APO L 0.5 W objective), with 50% laser power scanning 4 times, for 2 min in total (optimized before the experiments). The region of interest for photoconversion was selected in the stump region that extends until 270 μm from the edge of the wound). Photoconversion was performed in 3 consecutive days at 8, 25 and 49 h post-amputation (hpA) on the same larvae. Fins were imaged at 9 hpA after the first photoconversion, at 24 hpA and 48 hpA before the new photoconversions and finally at 72 hpA using 15% laser at 488 nm (green channel) and 20% laser at 561 nm (red channel).

2.2.8. Statistical analyses

Samples were split into experimental groups by randomization. The sample size estimation and the power of the statistical test were computed using GPower. A preliminary analysis was used to determine the necessary sample size N of a test given $\alpha < 0.05$, power $\beta = 0.80$. Then the effect size was determined. Groups include the number of independent values, and statistical analysis was done using these independent values. Graph Pad Prism 7 Software (San Diego, CA, USA) was used to construct graphs and analyse data in all figures. Specific statistical tests were used to evaluate the significance of differences between groups. The type of test used and p values are indicated for each graph in figure legends. The number of independent experiments (biological replicates) presented is indicated in the figure legends.

3. Results

3.1. Macrophages are recruited in a single wave during wound healing

Fin fold amputation at 3 days post-fertilization (dpf) provides a valuable system to study macrophage response to a wound [11]. We investigated the dynamics of macrophage recruitment during wound healing using an *in vivo* imaging approach. Several studies, including ours, have described the kinetic of recruitment of macrophages in the context of wounded fin fold [11,12,49]. However, none of them scrupulously reports the hour-by-hour infiltration of macrophages at the wound during the first 15 hours after wounding. The caudal fin folds of transgenic reporters for macrophages, *Tg(mfap4:mcherry-F),* were amputated at 3 dpf and macrophages at the wound were imaged from 1 to 15 hours post Amputation (hpA) using confocal microscopy. Quantification of macrophage recruitment during this period showed that macrophage number increased from 1 hpA to 8 hpA, then their number remained constant (Fig. S1). We also studied whether different waves of macrophages infiltrate the wound during healing or whether macrophages are recruited at once during early steps and then stay at the wound until the time of complete fin fold regeneration process. First we tracked recruited macrophages using, *Tg(mpeg1:Gal4/UAS:Kaede)* larvae, in which macrophages express the photoconvertible protein Kaede, allowing macrophages at the wound to be photoconverted from green to red upon UV illumination. We thus photoconverted macrophages at the wound at 8 hpA, a time point when most macrophages have reached the wound and we followed their localization during the whole regeneration process, *i.*e. 72 hpA (Fig. 1A). This approach allowed us to unambiguously recognize and follow macrophages that had been firstly recruited to the wound (photoconverted green macrophages) from those newly recruited (non-converted red macrophages) (Fig. 1B and movie 1).

Supplementary video related to this article can be found at https://doi.org/10.1016/j.freeradbiomed.2022.09.021

Using this approach, we performed series of pulse-chase photoconversion experiments and counted the number of red/green macrophages the day after to quantify the rate of "newly recruited" versus "firstly recruited" during the whole course of regeneration process (Fig. 1C). We found that the number of converted macrophages ("firstly recruited") at the wound was superior to the non-converted

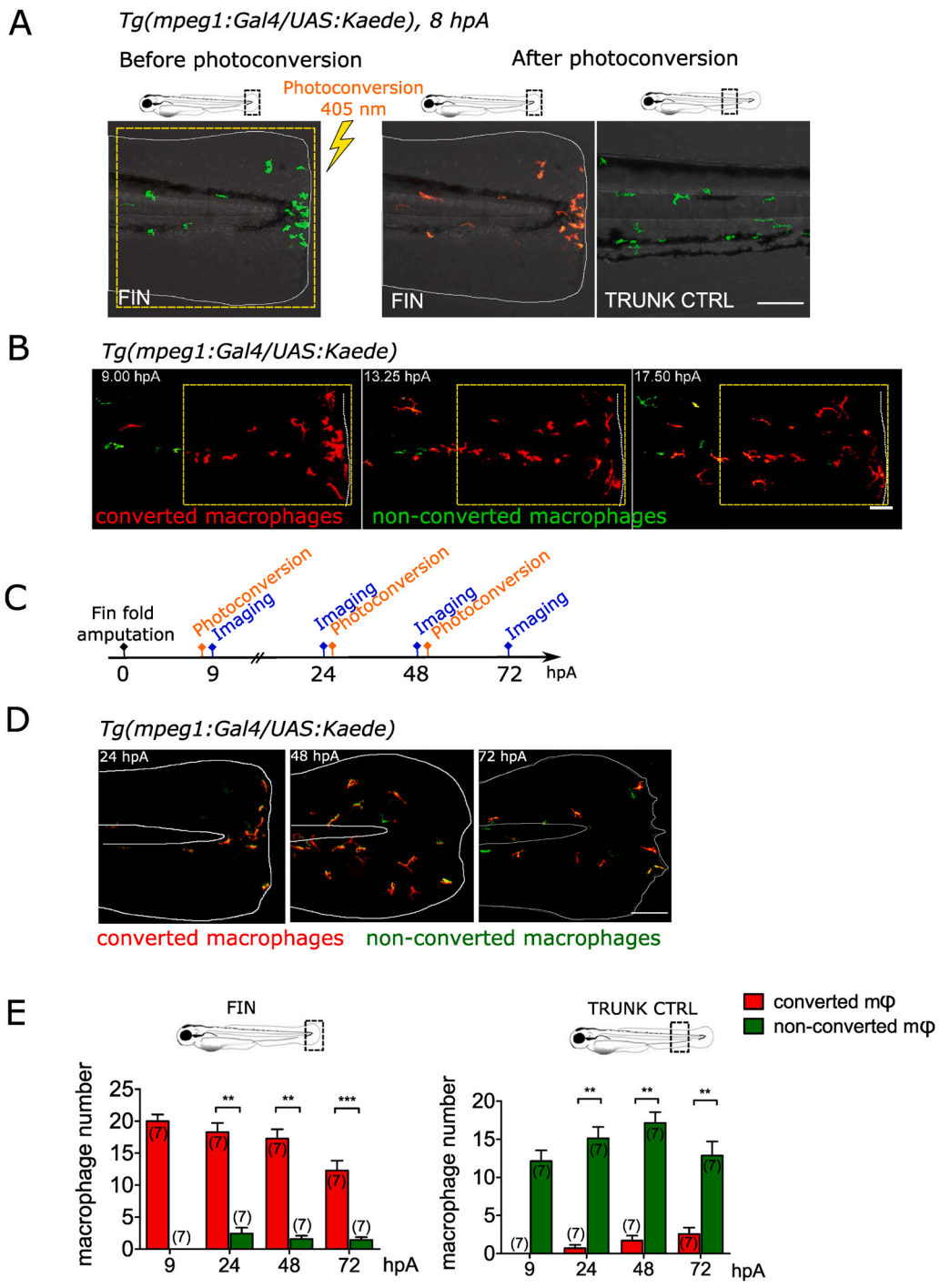

Fig. 1. Same population of macrophages is present at the wound during healing and repair **(A)** The caudal fin fold of *Tg(mpeg1:Gal4/UAS:Kaede)* larvae was amputated at 3 dpf. Recruited Kaede^{+} macrophages (green) were photo-converted to red fluorescence using UV at using 403 nm laser illumination in the wound region at 8 hpA. Representative confocal images of the fin fold before the photoconversion (left) and after the photoconversion (middle). On the right, control image of the trunk region taken after the photoconversion, outside of the wound area showing non-photoconverted macrophages (green). Representative merged images of the Kaede fluorescence in the green and red channels and bright field images. Yellow dashed line indicates the photoconverted area. The white lines outline the fin fold. Scale bar: 100 μm. **(B)** Representative frames (Maximum projection) of the time lapse imaging of photoconverted area, spanning from 9 to 19 hpA, with a time step of 10 min. White dashed line indicate the wound margin. Scale bar: 50 μm. **(C)** Schedule of the photoconversion pulse-chase experiment. Fin folds of *Tg(mpeg1:Gal4/UAS:Kaede)* larvae were amputated at 3 dpf. Photoconversions of Kaede^{+} macrophages were performed at 8, 25 and 49 hpA. Images were acquired at 9, 24, 48 and at 72 hpA. **(D)** Representative maximum projections of fin folds at 24, 48 and 72 hpA, taken before the new photoconversion; Merged images of the Kaede fluorescence (green and red channels). The white lines outline the fin fold and the notochord. Scale bar: 100 μm. **(E)** Quantification of photoconverted (red) and non-photoconverted (green) macrophages (Φ) at the wound (left) and in control trunk region (right), in indicated time point. Two independent experiments, number of larvae is indicated in the figure, Mann-Whitney test, two-tailed, $^{**}p < 0.01$, $^{***}p < 0.001$. (For interpretation of the references to colour in this figure legend, the reader is referred to the Web version of this article.)

macrophages and this number remained stable until 48 hpA and slightly decreased at 72 hpA. By contrast, very few non-converted macrophages ("newly recruited") were present at the wound every day (Fig. 1D). This was correlated with a low number of converted macrophages detected in the trunk region during regeneration, suggesting that very few "firstly recruited" macrophages leave the wound in later time points (Fig. 1E). These results indicate that most macrophages are recruited as a single wave immediately after the injury and remain associated to the wound over time. Only few wound-macrophages are newly recruited, suggesting that wound-macrophage phenotypes depend on intrinsic adaptation to changing environment rather than to recruitment of new macrophages.

3.1.1. *Macrophages undergo a stereotypical sequence of migratory behaviours during regeneration*

To describe the behaviour of macrophages during the regeneration process, we used wide-field real-time imaging of macrophage motility after caudal fin injury. Tracking individual macrophages during the whole regeneration in time-lapse video sequences is a challenging task because: 1/macrophages ultimately aggregate at the wound preventing us from differentiating the cells and their paths 2/continuous imaging of the amputated site in the same animal for several days is prevented by photobleaching and phototoxicity. To bypass these issues, we used *Tg (mpeg1:gal4/UAS:Kaede)* larvae in which the Kaede protein is strongly and mosaically expressed in macrophages, to enable long-time tracking of individual macrophages through the tissues without losing them.

Wound-macrophage motility was thus imaged by spinning disk confocal microscopy which is less biotoxic compared to classic confocal microscopy. The strategy was to prepare several groups of amputated larvae, and to image each group for one of consecutive periods lasting between 5 and 15 h, that together spanned 33 h of wound healing (Fig. 2A and B). Macrophage trajectory was then followed by manual tracking (Fig. 2B, bottom panel). Wide-field macrophage tracking analysis on whole larva confirmed that macrophages were recruited from peripheral tissues nearby the wound or from the Caudal Hematopoietic Tissue (CHT) (Fig. 2B, yellow square), while macrophages from more distant tissues were unaffected, like previously observed [50]. Unaffected macrophages of the truck region were thus used as internal controls (Fig. 2B, red square). Macrophage trajectory analysis at wound area revealed that during the period 1–6 hpA, they migrated directly towards the wound margin, with persistent directionality (Fig. 2C and movie 2

During the 6–20 hpA period, macrophages accumulated very close to

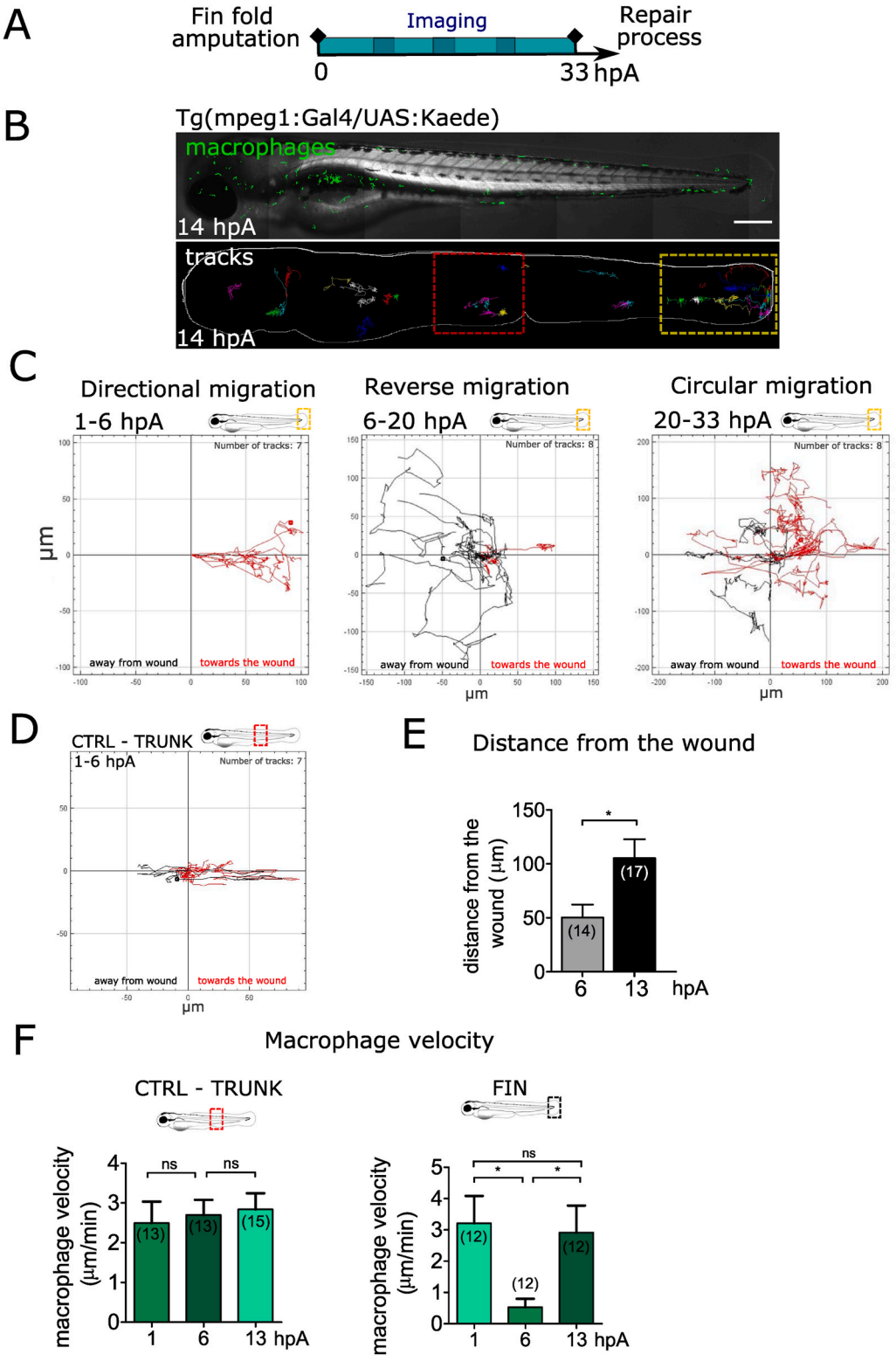

Fig. 2. *Macrophages undergo a stereotypical migratory behaviour at the wound* **(A)** Schedule of the experiments. *Tg (mpeg1:gal4/UAS:Kaede)* larvae with mosaic expression of Kaede protein in macrophages were amputated at 3 dpf and imaged using high resolution Spinning Disk microscopy for one of consecutive periods lasting between 5 and 15 h, that together spanned 72 h of regeneration spanning 3 days of regeneration. **(B)** Up: representative frame from 5.5 to 14 hpA time-lapse video of mosaically labelled macrophage population in the whole larva (14 hpA). Scale bar: 250 µm. Down: Representative tracks of macrophages representing the paths of individual macrophages from 5.5 to 14 hpA. **(C)** Macrophage migration directionality, in the wound region, during defined periods showing different migration modes: directional (period 1–6 hpA), reverse (period 6–20 hpA) and circular migration (period 20–33). The tracks with the directionality toward the wound are coloured in red, while the tracks with the directionality away from the wound are black. Number of macrophage tracks and the time period covered by graph are indicated above each graph. **(D)** Macrophage migration directionality in the unaffected trunk region (CTRL). The tracks with the directionality toward the wound are coloured in red, while the tracks with the directionality away from the wound are black. Number of macrophage tracks is indicated above the graph. **(E)** Quantification of wound distance value corresponding to the shortest distance measured from the wound margin to the center of each individual macrophage at 6 and 13 hpA. Number of macrophages is indicated in parenthesis. (mean±standard error of the min (sem)) Representative experiment of five independent experiments, two-tailed paired *t*-test, *p < 0.05. **(F)** Quantification of individual macrophage velocity at the control (CTRL) trunk region (left) and at the wound at 1, 6 and 13 hpA. Number of analysed macrophages is indicated in the graph. (mean±sem) Representative experiment of three independent experiments, two-tailed paired *t*-test, *p < 0.05, ns – not significant. (For interpretation of the references to colour in this figure legend, the reader is referred to the Web version of this article.)

the wound margin, reaching a peak around 6 hpA and lasting until 9 hpA (Fig. 2C and movie 3

After this point, macrophages started to reverse migrate away from the wound, with persistent directionality until 13–14 hpA before changing direction. During the 20–33 hpA period, macrophages displayed trajectories with frequent direction changes near to the wound area, with low persistence and alternating run phases and tumble that resulted in patrolling in the wound area (Fig. 2C and movie 4

Importantly, during these different periods, macrophages did not leave the wound area (Fig. 2C). The behaviour of wound-associated macrophages differed from non-activated macrophages present in unaffected trunk region (Fig. 2D).

The striking observation that macrophages switch behaviour after 9 hpA, prompted us to further analyse macrophage phenotype during that period. The position of macrophages at the wound can be quantified as a wound distance value, corresponding to the shortest distance between macrophage center and the wound margin. Wound distance values for individual macrophages present at the wound were calculated at 6 hpA (time point when macrophages are mainly accumulated at the wound) and 13 hpA (time point when macrophages change direction of their migration). The results showed significant increase in the average wound distance over time (Fig. 2E). While the velocity of non-activated macrophages in the CHT region remained constant over time (intrinsic control), macrophages being recruited had higher velocities in the initial phase (1 hpA), correlated with high directionality towards the wound. At 6 hpA, when macrophages accumulated at the wound margin, their velocity decreased dramatically. By contrast, at 13 hpA, reverse migrated macrophages had the same velocity as during the initial phase

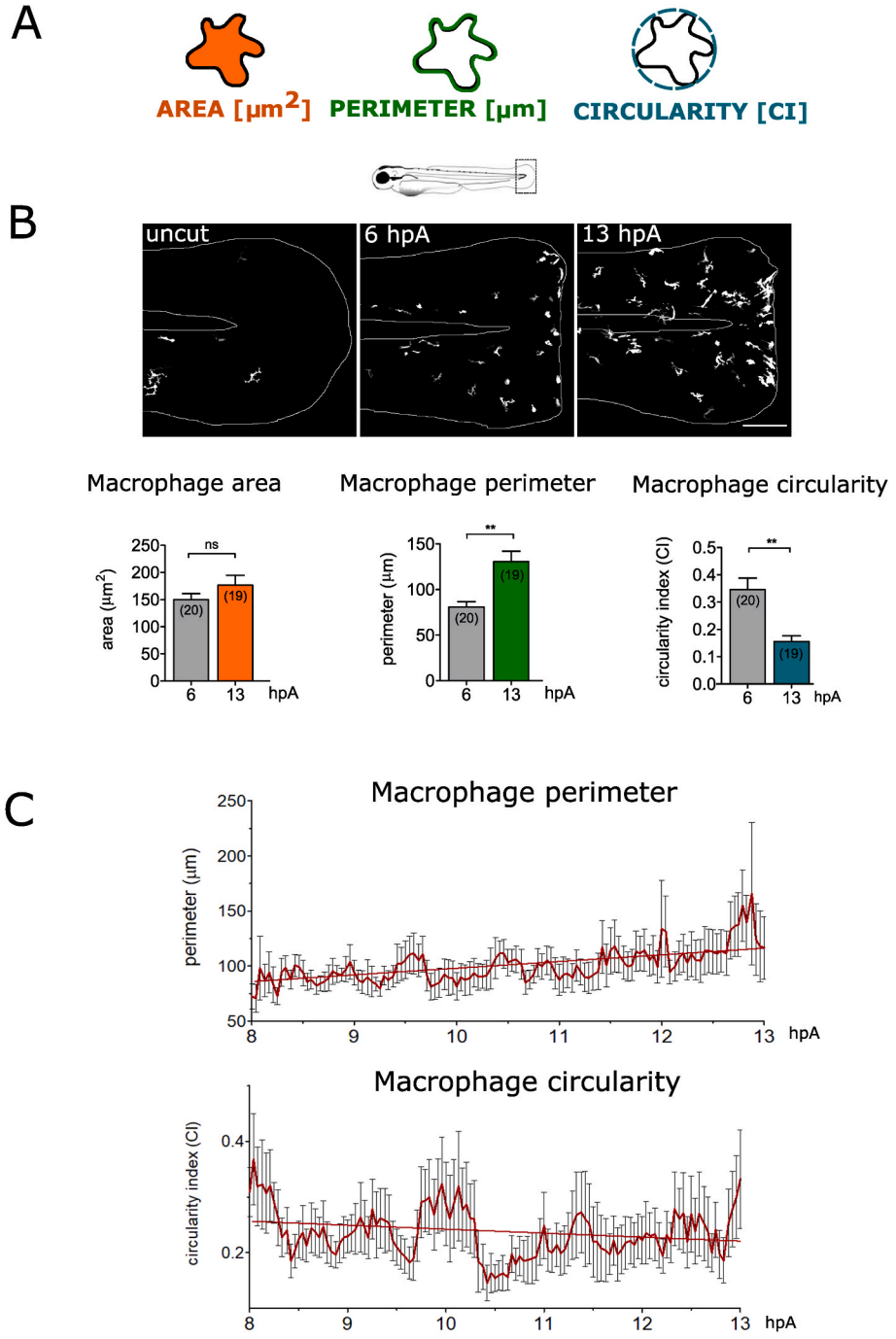

Fig. 3. *Macrophages change their morphology at the wound* **(A)** Representation of 2-D morphometric descriptors used for macrophage shape analysis: area, perimeter and circularity. **(B)** Up: Representative images of non-amputated and amputated fin folds of *Tg(mpeg1:Gal4/UAS:Kaede)* larvae at 6 and 13 hpA; confocal maximum projections of keade fluorescence (white) in macrophages. White lines outline the fin fold. Down: Quantification of area, perimeter and circularity for individual macrophages at 6 and 13 hpA. Number of analysed macrophages is indicated in parenthesis. (mean±sem) Representative experiment of five independent experiments, two-tailed paired *t*-test, $^{**}p < 0.01$, ns – not significant. **(C)** Quantification of perimeter (upper graph) and circularity value (lower graph) for individual macrophages present at the wound, during a time lapse sequence from 8 hpA to 13 hpA every 2.5 min (mean±sem).

(Fig. 2F).

Taken together, these results show that macrophages undergo a stereotypical set of migratory behaviours during wound healing. This behaviour of activated macrophages can be summarized as three main behaviours: directional migration to the wound, reverse migration from the wound and alternation of run and tumbling phases, occurring at conserved time windows in 3 dpf larvae.

3.1.2. Switch of macrophages behaviour correlate with changes in macrophage shape during wound healing

We hypothesised that changes in migration modes are a consequence of macrophage phenotype switch. Previously, differences in macrophages morphology have been associated with changes in pro-inflammatory and pro-healing state [23]. To test whether the switch of macrophage behaviour correlates with changes in macrophage morphology, we analysed the shape of individual macrophages in 2-D extracted from time lapse imaging of *Tg(mpeg1:gal4/UAS:Kaede)*. We described the 2-D macrophage shape through following morphometric descriptors: 1/area 2/perimeter 3/circularity. Higher circularity index (CI) indicates the amoeboid shape, while higher perimeter indicates the macrophage elongation and branching (Fig. 3A). Morphometric descriptor analysis at 6 hpA and 13 hpA revealed that, while macrophage area remained constant, macrophage perimeter significantly increased and, concomitantly, circularity decreased at 13 hpA, showing that macrophages change their shapes over time, from amoeboid/circular towards mesenchymal/branched type (Fig. 3B). In order to describe the dynamics of macrophage shape at the wound, we analysed the real time morphology of individual macrophages using time-lapse imaging every 3 min from 8 to 13 hpA to capture a large number of frames **(movie 5)**

An automated analysis applying the combination of the local Otsu and the SUBSURF method to the filtered images obtained by space-time filtering was used to identify and segment macrophages, and measure shape descriptors over the time. We showed that macrophage perimeter progressively increased over time while their circularity decreased, highlighting the changes of macrophage morphology from amoeboid to elongated shape (Fig. 3C). The morphology switch observed between 8 and 13 hpA thus occured concomitantly with the reverse migration and the change of the migration mode (from amoeboid to mesenchymal). High resolution imaging of wound macrophages using *Tg(mfap4:*

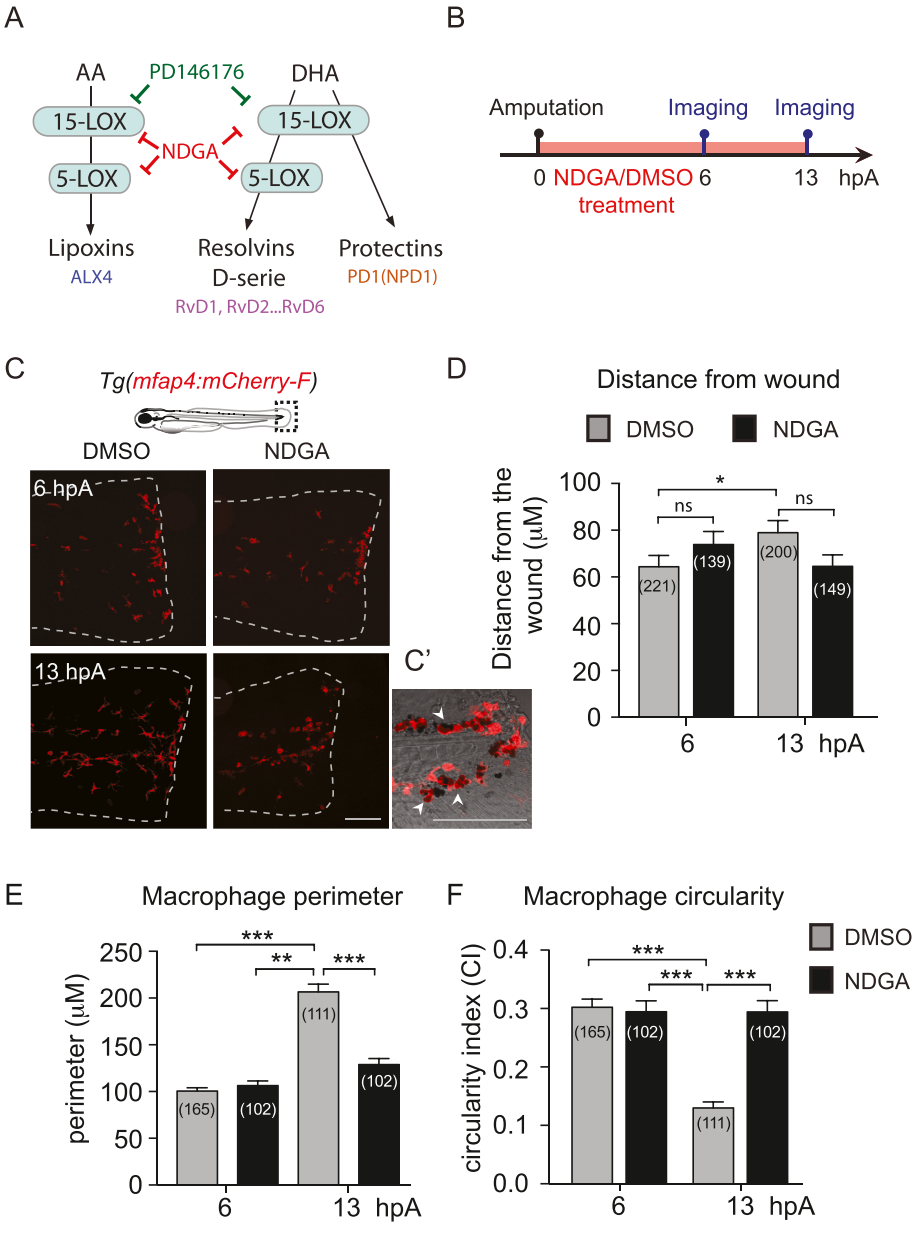

Fig. 4. Inhibition of Lipid metabolism via NDGA alters macrophage behavioural switch **(A)** The biosynthetic pathways of SPM leading to lipoxins, D-series resolvins and Protectins. Lipoxins (LXA4) are derived from arachidonic acid (AA) through the action of 15-Lipoxygenase (15-LOX) and Lipoxygenase 5 (5-LOX). D-series resolvins (RvD1 … 6) and protectins (PD1) are derived from docosahexaenoic acid (DHA) by the action 15-LOX and 5-LOX and from 15-LOX only, respectively. **(B)** Schedule of the experiment. The fin folds of *Tg(mfap4:mcherry-F)* larvae were amputated at 3 dpf and immediately treated with DMSO or NDGA 50 μM. Larvae were imaged in live at 6 and 13 hpA. **(C)** Representative images of the fin folds from amputated *Tg(mfap4:mcherry-F)* larvae at 13 hpA after DMSO or NDGA 50 μM treatment. Images are maximum projections from confocal microscopy showing the fluorescence of mCherry-F (macrophages) in the fin folds. White lines outline the fin fold. Scale bar: 100 μm. **(C')** Zoomed region of the wound at 13 hpA after NDGA 50 μM treatment. Maximum projection from confocal microscopy z-stack showing the fluorescence of mCherry-F (macrophages) overlaid on a brightfield image. Arrow heads show macrophages around pigments. Scale bar: 100 μm **(D)** Quantification of macrophage distance from the wound (values in μm) in DMSO or NDGA -treated larvae at 6 and 13 hpA. Mean±sem, three independent experiments, the number of analysed macrophages in parenthesis, kruskal-Wallis test with Dunn's post-test, ***$p < 0.001$, ns – not significant. **(E)** Quantification of macrophage perimeter in DMSO or NDGA -treated larvae at 6 and 13 hpA. Mean±sem, three independent experiments, the number of analysed macrophages is indicated in parenthesis, kruskal-Wallis test with Dunn's post-test, **$p < 0.01$, ***$p < 0.001$. **(F)** Quantification of macrophage circularity in DMSO or NDGA -treated larvae at 6 and 13 hpA. Mean±sem, three independent experiments, the number of analysed macrophages is indicated in parenthesis, kruskal-Wallis test with Dunn's post-test, ***$p < 0.001$.

mCherryF), another macrophage reporter line, and 3-D reconstructions of the surfaces at different time points after wounding revealed that at 6 h, macrophages were all morphologically spherical. At 9 hpA few macrophages started to have an irregular morphology and cells elongated with increasing number of cytoplasm extensions over time, until full mesenchymal morphology at 24 hpA (Fig. S2). These results suggest that macrophages undergo an extensive and specific behavioural and morphological switch that is concomitant to gene reprogramming during wound healing process.

3.1.3. *Lipid metabolic pathway regulates macrophage behavioural switch*

Specialized pro-resolving mediators (SPMs), including resolvins, maresins, protectins and lipoxins are a family of lipids that modulates the resolution phase of inflammation [25,51]. They are metabolites of omega-3 polyunsaturated fatty acids (PUFA) such as docosahexaenoic acid (DHA, C22:6 (n-3)) or omega-6 fatty acids such as arachidonic acid (AA, C20:4 (n-6)) and are produced by lipoxygenase (LOX)-driven pathways (Fig. 4-A). Previous work indicated that LOXs are important for macrophage function in mammals [52] and in zebrafish [35,53,54]. We checked whether LOX activity is involved in macrophage behaviour and morphology during wound healing. The fin fold of *Tg(mfap4:mCherryF)* larvae were wounded at 3 dpf and then treated immediately with 50 μM of the general LOX inhibitor nordihydroguaiaretic acid (NDGA) [55] (Fig. 4-B). No toxicity was detected in the NDGA treated larvae at this concentration (data not shown). Assessment of macrophage distance from the wound showed no significant differences in those distances between DMSO and NDGA groups at 6 and 13 hpA (Fig. 4C and D). However, NDGA treatment modified the position of macrophages which were localised at the level of the ventral and dorsal stipes of pigments in the tail, positioned around pigments, suggesting a phagocytic state (Fig. 4C').

The analysis of macrophage morphology revealed, that at 13 hpA NDGA treatment decreased the perimeter and increased the circularity of macrophages compared to the control condition (DMSO) (Fig. 4C,E-F), abolishing macrophages morphological changes occurring between 6 and 13 hpA, while at 6 hpA NDGA treatment did not affect macrophage perimeter and circularity compared to DMSO treatment. Importantly, we observed that NDGA treatment did not affect the number of recruited macrophages at 6 and 13 hpA compared to DMSO treatment (control) (Figure S3 A) or modify the global number of macrophages in the tail

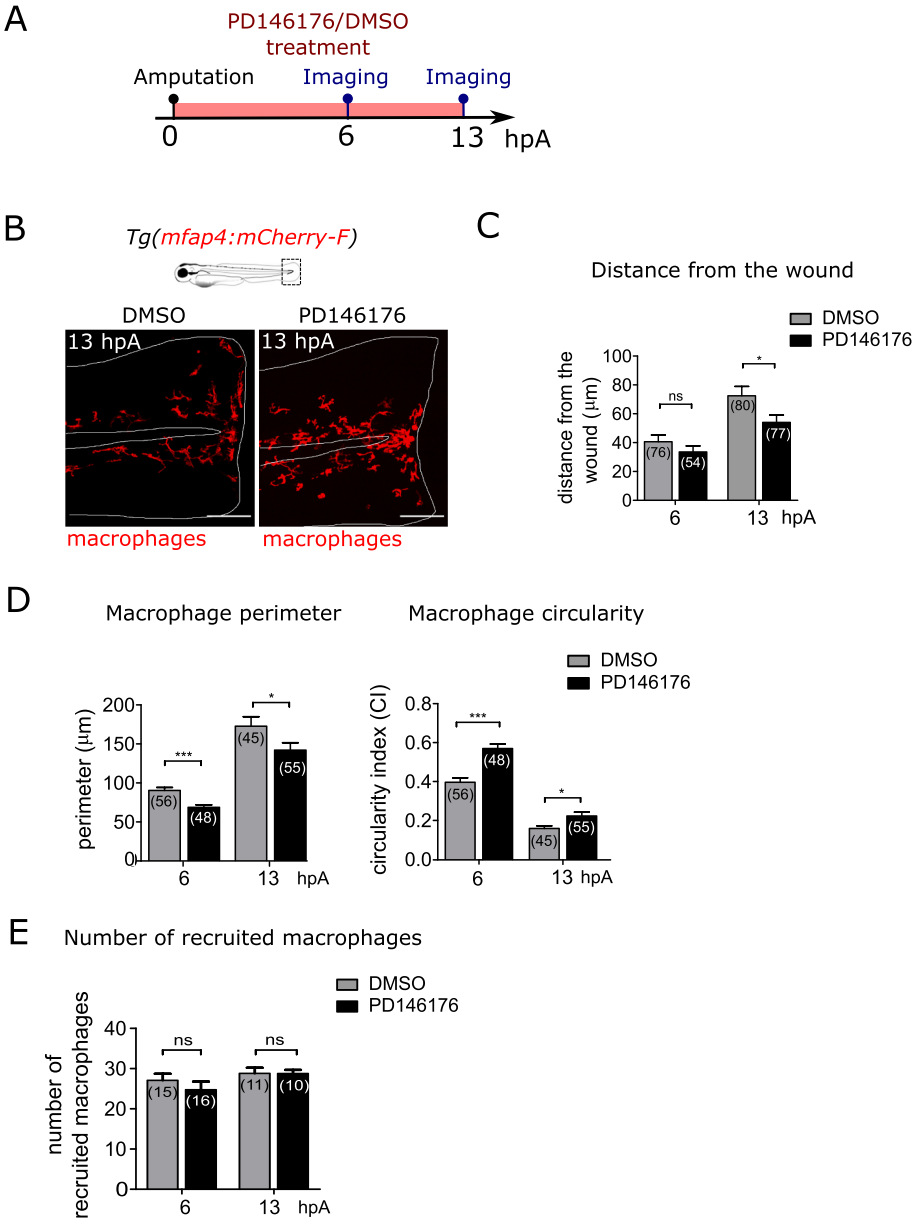

Fig. 5. Lipoxygenase 15 activity is required for macrophage behavioural switch **(A)** Schedule of the experiment. The fin folds of *Tg(mfap4:mcherry-F)* larvae were amputated at 3 dpf and immediately treated with DMSO or PD146176. Larvae were imaged in live at 6 and 13 hpA. **(B)** Representative images of the fin folds from amputated *Tg(mfap4:mcherry-F)* larvae at 13 hpA after DMSO or PD146176 treatment; Maximum projections from confocal microscopy showing mCherry-F macrophages in the fin folds. White lines outline the fin fold and the notochord. Scale bar: 100 μm. **(C)** Quantification of macrophage wound distance in DMSO- and PD146176-treated larvae at 6 and 13 hpA. Mean±sem, two independent experiments, the number of analysed macrophages from 4 larvae is indicated in parenthesis, two-tailed Mann-Whitney test, *$p < 0.05$, ns – not significant **(D)** Quantification of macrophage perimeter and circularity in DMSO- and PD146176-treated larvae at 6 and 13 hpA. Mean±sem, two independent experiments, number of analysed macrophages from 4 larvae is indicated in parenthesis, two-tailed Mann-Whitney test, *$p < 0.05$, ***$p < 0.001$. **(E)** Quantification of the number of recruited macrophages at 6 and 13 hpA, in DMSO- and PD146176-treated larvae. Mean±sem, two independent experiments, number of larvae is indicated in parenthesis. Two-tailed Mann-Whitney test, ns – not significant.

and the trunk (Figure S3 A). This result shows that global inhibition of LOX activity affects the morphological switch and the position of macrophages at the wound.

LOX enzymes are encoded by Alox genes. *alox5a*, *alox12*, *alox12b*, *alox15b* and *alox2* are expressed in the zebrafish larva [56,57]. Moreover zebrafish 15-LOX was suggested to be involved in neutrophil reverse migration [54]. The function of 15-LOX in macrophage behaviour and shape during wound healing remains unknown. We thus tested whether 15-LOX activity was important for macrophage behaviour using the specific 15-LOX inhibitor PD146176**.** To verify the efficacy of PD146176 treatment, we first treated the neutrophil reporter line, *Tg (mpx:GFP),* with 1.5 μM of PD146176 and confirmed that PD146176 treatment increased neutrophils number at the wound at 24 hpA (Fig. S4A), as previously reported [54]. Then, to follow the shape and the behaviour of macrophages, we treated *Tg(mfap4:mCherry-F)* larvae with PD146176 immediately after amputation and imaged macrophages at the wound at 6 and 13 hpA (Fig. 5A). While the position of macrophages related to the wound was unchanged at 6 hpA, macrophages were closer to the wound margin at 13 hpA in PD146176-treated larvae compared to controls (Fig. 5B), as shown by measurement of the distance from the wound (Fig. 5C). Further, macrophage perimeter was significantly lower compared to the DMSO control in both time points, while circularity was higher at 6 and 13 hpA (Fig. 5D), indicating that macrophage morphology was altered. Importantly, PD146176 treatment did not change the number of recruited macrophages neither at 6 hpA or at 13 hpA (Fig. 5E), or the global number of macrophages in treated larvae, compared to DMSO-treated controls (Fig. S3B). These data show that blocking the 15-LOX pathways alters the reverse migration of macrophages and impairs macrophage morphology, suggesting a role of the metabolites of 15-LOX pathways like lipoxin A4, D-series resolvin and protectin D1 (PD1) or intermediate products in this process.

Macrophages play key roles during regeneration processes [11–13]. To investigate whether the inhibition of 15-LOX activity affects the regeneration in zebrafish larvae, the caudal fin folds from wild type larvae were either kept intact (unwounded) or amputated (wounded) at 3 dpf. Subsequently larvae were treated with the general LOX inhibitor NDGA and imaged for regeneration measurement 3 days later (Figure S5 A). First, NDGA treatment did not change the development of the fin fold in unwounded larvae at 6 dpf compared to DMSO treatment (Figure S5 B). Second, NDGA treatment significantly reduced the fin fold regenerative growth in wounded larvae compared to DMSO, as measured as length or/and area from the initial amputation position to the new distal fin fold edge at 3 dpA (Fig. S5 B–C-D). Similar results were obtained with PD146176 treatment (Fig. S5 E-F), showing that 15-LOX inhibition impairs regeneration process.

3.1.4. Protectin D1, but not resolvin D1 enhances macrophage morphological and behavioural switch

Several SPMs including AA-derived-oxylipin LXA4 and DHA-derived D-series resolvin and protectin D1 (PD1) are produced via 15-LOX pathway [51,58–61] (Fig. 4 A). Interestingly, resolvin D1 (RvD1) and protectin D1 (PD1) were previously shown to regulate macrophage function. Resolvin D1 (RvD1) was shown to promotes macrophage polarization toward a M2 phenotype in cultured primary human macrophages [29,61] and in a liver ischemia/reperfusion injury model [62]. In the case of PD1, this SPM has an action on diabetic macrophage functions in diabetic wound healing in mice [63]. In addition, PD1 down regulates pro-inflammatory cytokines expression in LPS-activated human macrophages [27]. Recently we showed that treatment of zebrafish larvae with PD1 enhances the fin fold regeneration by acting through macrophages and promoting M2-like reprogramming [37]. Therefore, we decided to focus on resolvin D1 and protectin D1 and we investigated their role on macrophage behaviour during wound healing. To that end, a synthetic RvD1 was injected in the larvae intravenously. Having no information about the optimal dose of RvD1 in zebrafish larvae, the dose was determined based on our previous data showing that another SPM, PD1, has a pro-regenerative action in zebrafish with doses comprised between 40 and 400 pg. We thus decided to inject in the caudal vein of 3 dpf *Tg(mfap4:mCherry-F)* larvae a very high dose of RvD1, i.e. 450 pg, and then fin folds were amputated 1 h after this injection (Fig. S6A). Macrophage shape and behaviour were analysed by time-lapse imaging of the wound area from 5 to 13 hpA in RvD1-treated larvae and control larvae (Fig. S6B). RvD1-treated larvae showed no significant difference in macrophage wound distance at 9 and 13 hpA compared to controls (Fig. S6C). In addition, RvD1 did not modify the macrophage perimeter and circularity at 9, 11 and 13 hpA (Fig. S6D). These results suggest that RvD1 at high dose is not involved in macrophage behavioural switch at the wound.

To investigate the role of PD1 in macrophage behavioural switch, we injected an optimal dose of 200 pg of PD1 in the caudal vein of 3 dpf *Tg (mfap4:mCherry-F)* larvae, 1 h before the amputation (Fig. 6A) and analysed macrophage behaviour and morphology using time lapse imaging from 5 to 13 hpA. Macrophages were normally recruited to the wound, but their reverse migration was enhanced compared to the control (Fig. 6B and movie 6

Measuring the distance separating macrophages from the wound, we showed that the wound distance in PD1 treatment was similar to that of control at 6 hpA. However, the wound distance in PD1 treatment was dramatically higher at 9 hpA, while at 13 hpA it was similar to control again (Fig. 6C), due to expected reverse migration of macrophages in the control condition by that time. In addition, analysis of the shape factors at 6, 9, 11 and 13 hpA revealed that both the perimeter and circularity of macrophages in PD1 treated larvae were similar compared to the control at 6 hpA and 13 hpA. However, the perimeter was significantly increased at 9 and 11 hpA, while circularity was significantly decreased (Fig. 6D). These results reveal that PD1 stimulates the behavioural switch of macrophages.

To evaluate whether the effect of PD1 on macrophage behaviour is dose dependent, different doses of PD1 (100, 200, 400 pg) were injected in the caudal vein of 3 dpf *Tg(mfap4:mCherry-F)* larvae, 1 h before the amputation and the distance between macrophages and the wound was analysed using confocal microscopy at 9 hpA, a time point just prior the behavioural switch (Fig. S7). The result showed that increasing doses of PD1 caused different effects on macrophage wound distance (at 200 pg with $p = 0.0088$ and at 400 pg with $p = 0.0002$), showing that the effect of PD1 on macrophage behavior is dose-dependent. Similar experiment was performed using RvD1. Interestingly none of the tested doses of RvD1 (100, 200 pg or 400 pg) affected the macrophage behaviour, reinforcing the conclusion that RvD1 has no effect on macrophage motility (Fig. S7).

4. Discussion

A hallmark of macrophages is their high plasticity. Exploiting zebrafish advantages, we focused on the dynamics of behavioural patterns of individual macrophages in a changing wound microenvironment in a live animal. In this study, we used 4-D live imaging in zebrafish to record macrophage behaviour and shape, and demonstrate that the wound is colonized by a single wave of macrophages and that macrophages undergo dramatic changes in their shape and behaviour during healing. We show that this dynamic behaviour of wound-macrophages depends on lipid metabolism.

Upon injury, macrophages react rapidly to wound signals and phagocyte cellular debris, initiate inflammatory response and promote tissue remodeling and repair [2]. It was still unclear whether a single macrophage population is in charge of these different functions at the wound. Using photoconversion to unambiguously track macrophages infiltrating the wound region, we showed that macrophages are recruited in a single wave and that these wound-macrophages remain associated to the wound until the end of the regeneration. Very few macrophages are newly recruited after 8 hpA. Previously, we have

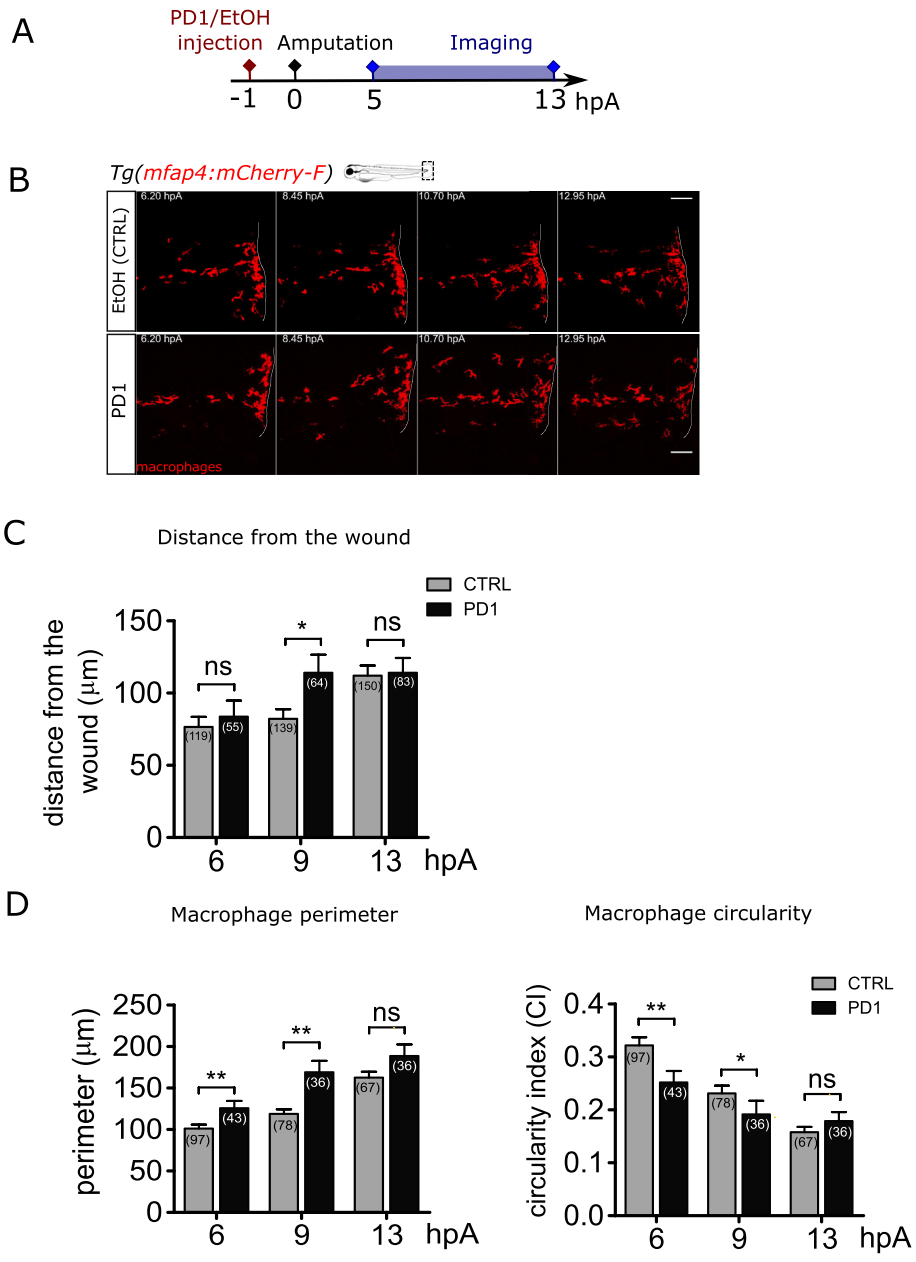

Fig. 6. Synthetic SPM protectin D1 accelerates the macrophage behavioural switch at the wound. **(A)** Schedule of the experiment. Protectin D1 (PD1) or same volume of ethanol were injected in 3 dpf *Tg (mfap4:mCherry-F)* larvae, 1 h before the fin fold amputation, and imaged from 5 to 13 hpA. **(B)** Representative frames of time-lapse imaging of *Tg (mfap4:mCherry-F)* larvae injected with ethanol as a control (up) or with PD1 (down). White lines indicate wound margin. Scale bars: 100 µm. **(C)** Quantification of macrophage distance from the wound margin in ethanol - (CTRL) and PD1-injected larvae at 6, 9, and 13 hpA. Number of macrophages is indicated in parenthesis. Mean±sem, from two independent experiments, two-tailed Mann Whitney test, $^{**}p < 0.01$, ns – not significant. **(D)** Quantification of macrophage perimeter and circularity in ethanol - (CTRL) and PD1-injected larvae at 6, 9, 10, 11, 12 and 13 hpA. Number of analysed macrophages is indicated in parenthesis; two independent experiments, Mann-Whitney two-tailed test, $^{*}p < 0.05$, $^{**}p < 0.01$ and $^{***}p < 0.01$.

shown that wound-macrophages reprogramed from M1-like phenotype, expressing pro-inflammatory genes like *tnfa*, *tnfb* and *il1b*, to M2-like phenotypes, expressing *tgfb1, ccr2* and *cxcr4* [36]. Our new finding strongly supports that the different macrophage phenotypes found at the wound mainly rely on a macrophage-intrinsic adaptation to changing environment rather than the recruitment of new macrophages.

Macrophage migration mode has been studied in real time and *in vivo* using different model systems [49,64,65]. We provide here an in-depth characterization of macrophage behavioural patterns and morphologies during the healing process. Using live imaging, trajectory analysis and shape descriptors, we showed that macrophages adopt series of stereotyped behaviours. First, macrophages undergo a high velocity directional migration, ending up in the accumulation at the wound of macrophages with low velocity and amoeboid shape. Second, between 9 and 13 hpA, macrophages undergo reverse migration, followed by a decrease of velocity and shape changes towards branched and elongated morphology. During the third phase macrophages undergo a circular migration using mesenchymal mode, with constant high velocity and displaying branched and elongated shape. This behavior continues untill the end of wound repair (Fig. 7). This pattern of migration is very similar to what has been observed within interstitial tissues in zebrafish, where unstimulated macrophages move using a Rac-dependent mesenchymal migration mode [64]. In addition, during later stages of wound healing response, zebrafish macrophages move randomly with a mesenchymal shape as murine macrophages in 3D matrices. This later process, which is dependent on β1 integrins has recently been proposed to be important for surveillance [66]. These results highlight the dynamics of behavioural patterns of macrophages in the versatile microenvironment of the wound. The extreme reactivity has also been observed in another context: during zebrafish hematopoiesis where macrophages constantly adapt, switching migratory shapes [67].

The zebrafish tail transection has emerged as a convenient model to study leukocytes reverse migration [54,68,69]. Here our goal was to identify which molecular mechanism regulates macrophage behavioural switch and reverse migration. An important finding in the present study is that Lipoxygenase (LOX) activity controls the switch of shape and

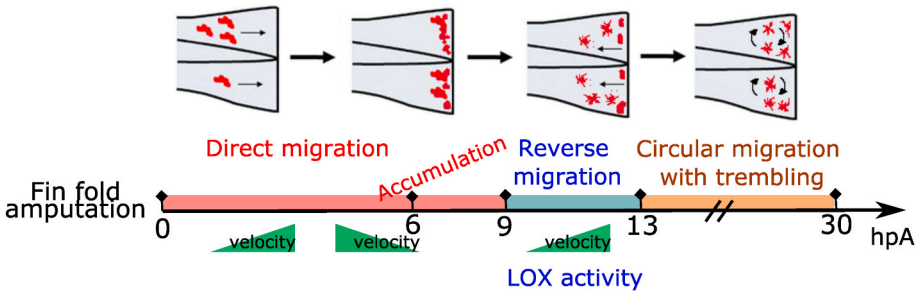

Fig. 7. Diagram of macrophage behavioural switch during wound healing Macrophage behavioural changes during wound healing highlighting 3 different migration modes, velocity changes and shape changes at indicated time points after amputation. First, macrophages undergo a directional migration, with high velocity, followed with accumulation of macrophages at the wound, having low velocity and amoeboid shape. Second macrophages undergo a reverse migration, with the opposite directionality compared to the first phase, occurring between 9 and 13 hpA. This phase also includes increase of velocity and shape changes towards branched, elongated morphology and it is regulated by LOX activity. The third phase is circular migration using mesenchymal mode, with constant high velocity and branched, elongated shape, lasting till the end of wound repair.

behaviour of macrophages during healing. Present in prokaryotes and eukaryotes [70], LOX enzymes do transform poly-unsaturated fatty acids into signaling molecules. Some of them like 12-LOX, 12/15-LOX and 5-LOX are expressed in leukocytes in mice and play important role in pathophysiology including inflammation, skin disorder, and tumorigenesis [71]. Here we deciphered the role of LOX activity using different pharmacological inhibitors: the pan inhibitor NDGA and PD146176, a specific inhibitor of 15-LOX activity. Our functional data conclude that both global and specific inhibition of LOX activity impair the morphology and the behaviour of macrophages. In addition, both LOX inhibitions lead to reduced growth of the regenerative fin fold, suggesting that LOX activity is necessary for tissue regeneration through the modulation of macrophage behaviour. Importantly, in our model, LOX inhibition with PD146176 does not affect macrophage migration toward the wound, nor does NDGA treatment. Recently, it has been reported that *alox12* knockdown reduces macrophage recruitment to the site of injury in both models of β cell injury and the tail injury [53]. This strongly suggests that more than one LOX enzyme contribute to the control of macrophage function at the wound. Collectively these data suggest an important role of LOX enzymes in tissue regeneration, probably through modulation of macrophage reactivity and adaptation to the microenvironment.

The metabolites of omega-3 polyunsaturated fatty acids (PUFAs) like docosahexaenoic acid (DHA) possess immunomodulatory properties [51] and may influence the outcome of wound healing [72]. Resolvin D1 and protectin D1, two 15-LOX derived DHA metabolites, were shown to be bioactive and to modulate macrophage functions [29,63,73]. In this study, we showed that protectin D1, but not Resolving D1, modifies the behaviour and shape of macrophages at the wound, favoring macrophage reverse migration, mesenchymal migration and elongated shape. This provides a potential explanation for how 15-LOX-dependent mechanism controls the behaviour and function of macrophages through the production of specific SPM like PD1. However it is not possible to assess whether it is PD1 itself or one of its derivatives which drives the effect, as metabolization of PD1 can be extremely rapid [74]. Recently, we showed that PD1 decreases the expression of some M1 markers and increases that of M2 markers after tail injury in zebrafish [37]. In accordance with our previous study, our new finding highlights the potency of PD1 in modulating macrophage function by deeply modifying their gene expression profiles, their morphology and behaviour, and accelerating the phenotype switch from pro-inflammatory M1-like toward M2-like phenotype.

Why PD1 controlled the behaviour and shape of macrophages at the wound while RvD1 did not? This could be due to differences in the availability of genuine receptors for PD1 versus RvD1 in zebrafish. Indeed, the G protein–coupled receptor (GPCRs), GPR37, was recently suggested to be the receptor of PD1. In murine macrophages, GPR37 activation though PD1 binding control cytokine production and regulate inflammation [75]. Two putative zebrafish *gpr37a* and *gpr37b* genes exist, however it is still unknown whether PD1 can signal through their encoded receptors. In mammalian leukocytes, RvD1 activity may be mediated by GPCRs, ALX/FPR2 and GPR32 [76,77]. In zebrafish, *formyl peptide receptor 2 (alx/fpr2)* and *gpr32* are not present although an ortholog of the close family member of Formyl peptide receptors, *FPR1* [78], exists. In the future, it will be important to identify the exact SPMs receptors active in zebrafish.

5. Conclusion

Challenged macrophages are remarkably plastic, changing their gene-expression program and function in healthy and diseased tissues. However, macrophages also constantly adapt to local cues, switching behaviour and shape in highly dynamic scenarios, such as during wound healing. Here, we capture the dynamics of macrophage recruitment and behaviour after caudal fin wounding in the transparent zebrafish larva. We showed that macrophages are recruited to the wound as a single wave where they switch their phenotype and that they display a highly stereotypical set of behaviours and change their shape from amoeboid to elongated shape as wound healing proceeds. Conceptually, the demonstration that this process is controlled by a 15-LOX-dependent mechanism, has important implications for targeting the polyunsaturated fatty acid metabolism to modulate macrophage behavior during pathological wounds or trauma in mammals.

Funding

This work has received funding from the European Union's Horizon 2020 research and innovation programme by the grant Marie-Curie Innovative Training Network ImageInLife: Grant Agreement n° 721,537 and the grant Marie Skłodowska-Curie ITN INFLANET: grant agreement n°955,576. This work was also supported by the Agence Nationale de la Recherche, France [ANR-19-CE15-0005-01, MacrophageDynamics], a grant from Region Occitanie, France (REPERE « INFLANET ») and the grant APVV-19-0460. Funding sources had no role in the writing of the manuscript or the decision to submit it for publication.

Declaration of competing interest

The authors declare they have no conflict of interest.

Acknowledgements

This work was undertaken with support from the fish facility of LPHI (University of Montpellier), and the qPCR Haut Debit platform of the University of Montpellier. We acknowledge the imaging facility BioCampus Montpellier Ressources Imagerie (MRI), member of the national infrastructure France-BioImaging supported by the French National Research Agency (ANR-10-INSB-04, "Investments for the future").

Appendix A. Supplementary data

Supplementary data to this article can be found online at https://doi.org/10.1016/j.freeradbiomed.2022.09.021.

References

[1] K.J. Sonnemann, W.M. Bement, Wound repair: toward understanding and integration of single-cell and multicellular wound responses, Annu. Rev. Cell Dev. Biol. 27 (2011) 237–263, https://doi.org/10.1146/annurev-cellbio-092910-154251.

[2] M. Hesketh, K.B. Sahin, Z.E. West, R.Z. Murray, Macrophage phenotypes regulate scar formation and chronic wound healing, Indian J. Manag. Sci. 18 (2017) 1545, https://doi.org/10.3390/ijms18071545.

[3] I. Goren, N. Allmann, N. Yogev, C. Schürmann, A. Linke, M. Holdener, A. Waisman, J. Pfeilschifter, S. Frank, A transgenic mouse model of inducible macrophage depletion, Am. J. Pathol. 175 (2009) 132–147, https://doi.org/10.2353/ajpath.2009.081002.

[4] S.J. Leibovich, R. Ross, The role of the macrophage in wound repair. A study with hydrocortisone and antimacrophage serum, Am. J. Pathol. 78 (1975) 71–100.

[5] T. Lucas, A. Waisman, R. Ranjan, J. Roes, T. Krieg, W. Müller, A. Roers, S.A. Eming, Differential roles of macrophages in diverse phases of skin repair, J. Immunol. 184 (2010) 3964–3977, https://doi.org/10.4049/jimmunol.0903356.

[6] L. Arnold, A. Henry, F. Poron, Y. Baba-Amer, N. van Rooijen, A. Plonquet, R. K. Gherardi, B. Chazaud, Inflammatory monocytes recruited after skeletal muscle injury switch into antiinflammatory macrophages to support myogenesis, J. Exp. Med. 204 (2007) 1057–1069, https://doi.org/10.1084/jem.20070075.

[7] J.S. Duffield, S.J. Forbes, C.M. Constandinou, S. Clay, M. Partolina, S. Vuthoori, S. Wu, R. Lang, J.P. Iredale, Selective depletion of macrophages reveals distinct, opposing roles during liver injury and repair, J. Clin. Invest. 115 (2005) 56–65, https://doi.org/10.1172/JCI200522675.

[8] J. Simkin, T.R. Gawriluk, J.C. Gensel, A.W. Seifert, Macrophages are necessary for epimorphic regeneration in African spiny mice, Elife 6 (2017), e24623, https://doi.org/10.7554/eLife.24623.

[9] J.W. Godwin, A.R. Pinto, N.A. Rosenthal, Macrophages are required for adult salamander limb regeneration, Proc. Natl. Acad. Sci. U.S.A. 110 (2013) 9415–9420, https://doi.org/10.1073/pnas.1300290110.

[10] T. Hasegawa, C.J. Hall, P.S. Crosier, G. Abe, K. Kawakami, A. Kudo, A. Kawakami, Transient inflammatory response mediated by interleukin-1β is required for proper regeneration in zebrafish fin fold, Elife 6 (2017), https://doi.org/10.7554/eLife.22716.

[11] V. Miskolci, J. Squirrell, J. Rindy, W. Vincent, J.D. Sauer, A. Gibson, K.W. Eliceiri, A. Huttenlocher, Distinct inflammatory and wound healing responses to complex caudal fin injuries of larval zebrafish, Elife 8 (2019), e45976, https://doi.org/10.7554/eLife.45976.

[12] M. Nguyen-Chi, B. Laplace-Builhé, J. Travnickova, P. Luz-Crawford, G. Tejedor, G. Lutfalla, K. Kissa, C. Jorgensen, F. Djouad, TNF signaling and macrophages govern fin regeneration in zebrafish larvae, Cell Death Dis. 8 (2017), https://doi.org/10.1038/cddis.2017.374 e2979–e2979.

[13] T.A. Petrie, N.S. Strand, C. Tsung-Yang, J.S. Rabinowitz, R.T. Moon, Macrophages modulate adult zebrafish tail fin regeneration, Development 141 (2014) 2581–2591, https://doi.org/10.1242/dev.098459.

[14] J.M. Daley, S.K. Brancato, A.A. Thomay, J.S. Reichner, J.E. Albina, The phenotype of murine wound macrophages, J. Leukoc. Biol. 87 (2010) 59–67, https://doi.org/10.1189/jlb.0409236.

[15] F. Ginhoux, J.L. Schultze, P.J. Murray, J. Ochando, S.K. Biswas, New insights into the multidimensional concept of macrophage ontogeny, activation and function, Nat. Immunol. 17 (2016) 34–40, https://doi.org/10.1038/ni.3324.

[16] A. Sica, A. Mantovani, Macrophage plasticity and polarization: in vivo veritas, J. Clin. Invest. 122 (2012) 787–795, https://doi.org/10.1172/JCI59643.

[17] K. Klinkert, D. Whelan, A.J.P. Clover, A.-L. Leblond, A.H.S. Kumar, N.M. Caplice, Selective M2 macrophage depletion leads to prolonged inflammation in surgical wounds, Eur. Surg. Res. 58 (2017) 109–120, https://doi.org/10.1159/000451078.

[18] P. Pelegrin, A. Surprenant, Dynamics of macrophage polarization reveal new mechanism to inhibit IL-1β release through pyrophosphates, EMBO J. 28 (2009) 2114–2127, https://doi.org/10.1038/emboj.2009.163.

[19] E.J. Vereyken, P.D. Heijnen, W. Baron, E.H. de Vries, C.D. Dijkstra, C.E. Teunissen, Classically and alternatively activated bone marrow derived macrophages differ in cytoskeletal functions and migration towards specific CNS cell types, J. Neuroinflammation 8 (2011) 58, https://doi.org/10.1186/1742-2094-8-58.

[20] F. Rey-Giraud, M. Hafner, C.H. Ries, In vitro generation of monocyte-derived macrophages under serum-free conditions improves their tumor promoting functions, PLoS One 7 (2012), e42656, https://doi.org/10.1371/journal.pone.0042656.

[21] C. Cougoule, E. Van Goethem, V. Le Cabec, F. Lafouresse, L. Dupré, V. Mehraj, J.-L. Mège, C. Lastrucci, I. Maridonneau-Parini, Blood leukocytes and macrophages of various phenotypes have distinct abilities to form podosomes and to migrate in 3D environments, Eur. J. Cell Biol. 91 (2012) 938–949, https://doi.org/10.1016/j.ejcb.2012.07.002.

[22] E. Van Goethem, R. Poincloux, F. Gauffre, I. Maridonneau-Parini, V. Le Cabec, Matrix architecture dictates three-dimensional migration modes of human macrophages: differential involvement of proteases and podosome-like structures, J. Inf. 184 (2010) 1049–1061, https://doi.org/10.4049/jimmunol.0902223.

[23] F.Y. McWhorter, T. Wang, P. Nguyen, T. Chung, W.F. Liu, Modulation of macrophage phenotype by cell shape, Proc. Natl. Acad. Sci. USA 110 (2013) 17253–17258, https://doi.org/10.1073/pnas.1308887110.

[24] N. Chiang, C.N. Serhan, Specialized pro-resolving mediator network: an update on production and actions, Essays Biochem. 64 (2020) 443–462, https://doi.org/10.1042/EBC20200018.

[25] S.C. Dyall, L. Balas, N.G. Bazan, J.T. Brenna, N. Chiang, F. da Costa Souza, J. Dalli, T. Durand, J.-M. Galano, P.J. Lein, et al., Polyunsaturated fatty acids and fatty acid-derived lipid mediators: recent advances in the understanding of their biosynthesis, structures, and functions, Prog. Lipid Res. 86 (2022), 101165, https://doi.org/10.1016/j.plipres.2022.101165.

[26] C.N. Serhan, Pro-resolving lipid mediators are leads for resolution physiology, Nature 510 (2014) 92–101, https://doi.org/10.1038/nature13479.

[27] R. Bosviel, L. Joumard-Cubizolles, G. Chinetti-Gbaguidi, D. Bayle, C. Copin, N. Hennuyer, I. Duplan, B. Staels, G. Zanoni, A. Porta, et al., DHA-derived oxylipins, neuroprostanes and protectins, differentially and dose-dependently modulate the inflammatory response in human macrophages: putative mechanisms through PPAR activation, Free Radic. Biol. Med. 103 (2017) 146–154, https://doi.org/10.1016/j.freeradbiomed.2016.12.018.

[28] J. Dalli, C.N. Serhan, Pro-resolving mediators in regulating and conferring macrophage function, Front. Immunol. 8 (2017) 1400, https://doi.org/10.3389/fimmu.2017.01400.

[29] M. Schmid, C. Gemperle, N. Rimann, M. Hersberger, Resolvin D1 polarizes primary human macrophages toward a proresolution phenotype through GPR32, J. Inf. 196 (2016) 3429–3437, https://doi.org/10.4049/jimmunol.1501701.

[30] J. Yuan, F. Lin, L. Chen, W. Chen, X. Pan, Y. Bai, Y. Cai, H. Lu, Lipoxin A4 regulates M1/M2 macrophage polarization via FPR2-IRF pathway, Inflammopharmacology 30 (2022) 487–498, https://doi.org/10.1007/s10787-022-00942-y.

[31] P. Herbomel, B. Thisse, C. Thisse, Ontogeny and behaviour of early macrophages in the zebrafish embryo, Development 126 (1999) 3735–3745.

[32] A. Sanz-Morejón, A.B. García-Redondo, H. Reuter, I.J. Marques, T. Bates, M. Galardi-Castilla, A. Große, S. Manig, X. Langa, A. Ernst, et al., Wilms tumor 1b expression defines a pro-regenerative macrophage subtype and is required for organ regeneration in the zebrafish, Cell Rep. 28 (2019) 1296–1306, https://doi.org/10.1016/j.celrep.2019.06.091, e6.

[33] J. Rougeot, V. Torraca, A. Zakrzewska, Z. Kanwal, H.J. Jansen, F. Sommer, H. P. Spaink, A.H. Meijer, RNAseq profiling of leukocyte populations in zebrafish larvae reveals a cxcl11 chemokine gene as a marker of macrophage polarization during mycobacterial infection, Front. Immunol. 10 (2019) 832, https://doi.org/10.3389/fimmu.2019.00832.

[34] F. Ellett, L. Pase, J.W. Hayman, A. Andrianopoulos, G.J. Lieschke, mpeg1 promoter transgenes direct macrophage-lineage expression in zebrafish, Blood 117 (2011) e49–e56, https://doi.org/10.1182/blood-2010-10-314120.

[35] A. Lewis, P.M. Elks, Hypoxia induces macrophage tnfa expression via cyclooxygenase and prostaglandin E2 in vivo, Front. Immunol. 10 (2019) 2321, https://doi.org/10.3389/fimmu.2019.02321.

[36] M. Nguyen-Chi, B. Laplace-Builhe, J. Travnickova, P. Luz-Crawford, G. Tejedor, Q. T. Phan, I. Duroux-Richard, J.-P. Levraud, K. Kissa, G. Lutfalla, et al., Identification of polarized macrophage subsets in zebrafish, Elife 4 (2015), e07288, https://doi.org/10.7554/eLife.07288.

[37] M. Nguyen-Chi, P. Luz-Crawford, L. Balas, T. Sipka, R. Contreras-López, A. Barthelaix, G. Lutfalla, T. Durand, C. Jorgensen, F. Djouad, Pro-resolving mediator protectin D1 promotes epimorphic regeneration by controlling immune cell function in vertebrates, Br. J. Pharmacol. 177 (2020) 4055–4073, https://doi.org/10.1111/bph.15156.

[38] Q.T. Phan, T. Sipka, C. Gonzalez, J.-P. Levraud, G. Lutfalla, M. Nguyen-Chi, Neutrophils use superoxide to control bacterial infection at a distance, PLoS Pathog. 14 (2018), e1007157, https://doi.org/10.1371/journal.ppat.1007157.

[39] S.A. Renshaw, C.A. Loynes, D.M.I. Trushell, S. Elworthy, P.W. Ingham, M.K. B. Whyte, A transgenic zebrafish model of neutrophilic inflammation, Blood 108 (2006) 3976–3978, https://doi.org/10.1182/blood-2006-05-024075.

[40] K. Hatta, H. Tsujii, T. Omura, Cell tracking using a photoconvertible fluorescent protein, Nat. Protoc. 1 (2006) 960–967, https://doi.org/10.1038/nprot.2006.96.

[41] C.B. Kimmel, W.W. Ballard, S.R. Kimmel, B. Ullmann, T.F. Schilling, Stages of embryonic development of the zebrafish, Dev. Dynam. 203 (1995) 253–310, https://doi.org/10.1002/aja.1002030302.

[42] G. Dayaker, T. Durand, L. Balas, A versatile and stereocontrolled total synthesis of dihydroxylated docosatrienes containing a conjugated *E,E,Z* -triene, Chem. Eur J. 20 (2014) 2879–2887, https://doi.org/10.1002/chem.201304526.

[43] H.S. Jónasdóttir, C. Papan, S. Fabritz, L. Balas, T. Durand, I. Hardardottir, J. Freysdottir, M. Giera, Differential mobility separation of leukotrienes and protectins, Anal. Chem. 87 (2015) 5036–5040, https://doi.org/10.1021/acs.analchem.5b00786.

[44] T. Sipka, R. Peroceschi, R. Hassan-Abdi, M. Groß, F. Ellett, C. Begon-Pescia, C. Gonzalez, G. Lutfalla, M. Nguyen-Chi, Damage-induced calcium signaling and reactive oxygen species mediate macrophage activation in zebrafish, Front. Immunol. 12 (2021), 636585, https://doi.org/10.3389/fimmu.2021.636585.

[45] A. Sarti, K. Mikula, F. Sgallari, Nonlinear multiscale analysis of three-dimensional echocardiographic sequences, IEEE Trans. Med. Imag. 18 (1999) 453–466, https://doi.org/10.1109/42.781012.

[46] N. Otsu, A threshold selection method from gray-level histograms, IEEE Trans. Syst., Man, Cybern. 9 (1979) 62–66, https://doi.org/10.1109/TSMC.1979.4310076.

[47] K. Saddami, K. Munadi, Y. Away, F. Arnia, Improvement of binarization performance using local otsu thresholding, Int. J. Energy a Clean Environ. (IJECE) 9 (2019) 264, https://doi.org/10.11591/ijece.v9i1.pp264-272.

[48] A. Sarti, R. Malladi, J.A. Sethian, Subjective surfaces: a method for completing missing boundaries, Proc. Natl. Acad. Sci. U.S.A. 97 (2000) 6258–6263, https://doi.org/10.1073/pnas.110135797.
[49] W. Hu, L. van Steijn, C. Li, F.J. Verbeek, L. Cao, R.M.H. Merks, H.P. Spaink, A novel function of TLR2 and MyD88 in the regulation of leukocyte cell migration behavior during wounding in zebrafish larvae, Front. Cell Dev. Biol. 9 (2021), 624571, https://doi.org/10.3389/fcell.2021.624571.
[50] R.A. Morales, M.L. Allende, Peripheral macrophages promote tissue regeneration in zebrafish by fine-tuning the inflammatory response, Front. Immunol. 10 (2019) 253, https://doi.org/10.3389/fimmu.2019.00253.
[51] C.D. Buckley, D.W. Gilroy, C.N. Serhan, Proresolving lipid mediators and mechanisms in the resolution of acute inflammation, Immunity 40 (2014) 315–327, https://doi.org/10.1016/j.immuni.2014.02.009.
[52] K. Pistorius, P.R. Souza, R. De Matteis, S. Austin-Williams, K.G. Primdahl, A. Vik, F. Mazzacuva, R.A. Colas, R.M. Marques, T.V. Hansen, et al., PDn-3 DPA pathway regulates human monocyte differentiation and macrophage function, Cell Chemical Biology 25 (2018) 749–760, https://doi.org/10.1016/j.chembiol.2018.04.017, e9.
[53] A. Kulkarni, A.R. Pineros, M.A. Walsh, I. Casimiro, S. Ibrahim, M. Hernandez-Perez, K.S. Orr, L. Glenn, J.L. Nadler, M.A. Morris, et al., 12-Lipoxygenase governs the innate immune pathogenesis of islet inflammation and autoimmune diabetes, JCI Insight 6 (2021), e147812, https://doi.org/10.1172/jci.insight.147812.
[54] C.A. Loynes, J.A. Lee, A.L. Robertson, M.J.G. Steel, F. Ellett, Y. Feng, B.D. Levy, M. K.B. Whyte, S.A. Renshaw, PGE $_2$ production at sites of tissue injury promotes an anti-inflammatory neutrophil phenotype and determines the outcome of inflammation resolution in vivo, Sci. Adv. 4 (2018) eaar8320, https://doi.org/10.1126/sciadv.aar8320.
[55] J. Van Wauwe, J. Goossens, Effects of antioxidants on cyclooxygenase and lipoxygenase activities in intact human platelets: comparison with indomethacin and etya, Prostaglandins 26 (1983) 725–730, https://doi.org/10.1016/0090-6980(83)90057-6.
[56] S. Adel, D. Heydeck, H. Kuhn, C. Ufer, The lipoxygenase pathway in zebrafish. Expression and characterization of zebrafish ALOX5 and comparison with its human ortholog, Biochim. Biophys. Acta Mol. Cell Biol. Lipids 1861 (2016) 1–11, https://doi.org/10.1016/j.bbalip.2015.10.001.
[57] A. Chatzopoulou, J.P.M. Heijmans, E. Burgerhout, N. Oskam, H.P. Spaink, A. H. Meijer, M.J.M. Schaaf, Glucocorticoid-induced attenuation of the inflammatory response in zebrafish, Endocrinology 157 (2016) 2772–2784, https://doi.org/10.1210/en.2015-2050.
[58] L. Balas, T. Durand, Dihydroxylated E,E,Z-docosatrienes. An overview of their synthesis and biological significance, Prog. Lipid Res. 61 (2016) 1–18, https://doi.org/10.1016/j.plipres.2015.10.002.
[59] L. Balas, M. Guichardant, T. Durand, M. Lagarde, Confusion between protectin D1 (PD1) and its isomer protectin DX (PDX). An overview on the dihydroxy-docosatrienes described to date, Biochimie 99 (2014) 1–7, https://doi.org/10.1016/j.biochi.2013.11.006.
[60] T.V. Hansen, A. Vik, C.N. Serhan, The protectin family of specialized pro-resolving mediators: potent immunoresolvents enabling innovative approaches to target obesity and diabetes, Front. Pharmacol. 9 (2019) 1582, https://doi.org/10.3389/fphar.2018.01582.
[61] S. Hong, K. Gronert, P.R. Devchand, R.-L. Moussignac, C.N. Serhan, Novel docosatrienes and 17S-resolvins generated from docosahexaenoic acid in murine brain, human blood, and glial cells, J. Biol. Chem. 278 (2003) 14677–14687, https://doi.org/10.1074/jbc.M300218200.
[62] J.-W. Kang, S.-M. Lee, Resolvin D1 protects the liver from ischemia/reperfusion injury by enhancing M2 macrophage polarization and efferocytosis, Biochim. Biophys. Acta Mol. Cell Biol. Lipids 1861 (2016) 1025–1035, https://doi.org/10.1016/j.bbalip.2016.06.002.
[63] S. Hong, H. Tian, Y. Lu, J.M. Laborde, F.A. Muhale, Q. Wang, B.V. Alapure, C. N. Serhan, N.G. Bazan, Neuroprotectin/protectin D1: endogenous biosynthesis and actions on diabetic macrophages in promoting wound healing and innervation impaired by diabetes, Am. J. Physiol. Cell Physiol. 307 (2014) C1058–C1067, https://doi.org/10.1152/ajpcell.00270.2014.
[64] F. Barros-Becker, P.-Y. Lam, R. Fisher, A. Huttenlocher, Live imaging reveals distinct modes of neutrophil and macrophage migration within interstitial tissues, Journal of Cell Science jcs (2017), 206128, https://doi.org/10.1242/jcs.206128.
[65] E.E. Rosowski, Q. Deng, N.P. Keller, A. Huttenlocher, Rac2 functions in both neutrophils and macrophages to mediate motility and host defense in larval zebrafish, J. Inf. 197 (2016) 4780–4790, https://doi.org/10.4049/jimmunol.1600928.
[66] N. Paterson, T. Lämmermann, Macrophage network dynamics depend on haptokinesis for optimal local surveillance, Elife 11 (2022), e75354, https://doi.org/10.7554/eLife.75354.
[67] J. Travnickova, S. Nhim, N. Abdellaoui, F. Djouad, M. Nguyen-Chi, A. Parmeggiani, K. Kissa, Macrophage morphological plasticity and migration is Rac signalling and MMP9 dependant, Sci. Rep. 11 (2021), 10123, https://doi.org/10.1038/s41598-021-88961-7.
[68] P.M. Elks, F.J. van Eeden, G. Dixon, X. Wang, C.C. Reyes-Aldasoro, P.W. Ingham, M.K.B. Whyte, S.R. Walmsley, S.A. Renshaw, Activation of hypoxia-inducible factor-1α (Hif-1α) delays inflammation resolution by reducing neutrophil apoptosis and reverse migration in a zebrafish inflammation model, Blood 118 (2011) 712–722, https://doi.org/10.1182/blood-2010-12-324186.
[69] J.R. Mathias, B.J. Perrin, T.-X. Liu, J. Kanki, A.T. Look, A. Huttenlocher, Resolution of inflammation by retrograde chemotaxis of neutrophils in transgenic zebrafish, J. Leukoc. Biol. 80 (2006) 1281–1288, https://doi.org/10.1189/jlb.0506346.
[70] J. Hansen, A. Garreta, M. Benincasa, M.C. Fusté, M. Busquets, A. Manresa, Bacterial lipoxygenases, a new subfamily of enzymes? A phylogenetic approach, Appl. Microbiol. Biotechnol. 97 (2013) 4737–4747, https://doi.org/10.1007/s00253-013-4887-9.
[71] R. Mashima, T. Okuyama, The role of lipoxygenases in pathophysiology; new insights and future perspectives, Redox Biol. 6 (2015) 297–310, https://doi.org/10.1016/j.redox.2015.08.006.
[72] Y. Lu, H. Tian, S. Hong, Novel 14,21-dihydroxy-docosahexaenoic acids: structures, formation pathways, and enhancement of wound healing, JLR (J. Lipid Res.) 51 (2010) 923–932, https://doi.org/10.1194/jlr.M000059.
[73] E. Titos, B. Rius, A. González-Périz, C. López-Vicario, E. Morán-Salvador, M. Martínez-Clemente, V. Arroyo, J. Clària, Resolvin D1 and its precursor docosahexaenoic acid promote resolution of adipose tissue inflammation by eliciting macrophage polarization toward an M2-like phenotype, J. Inf. 187 (2011) 5408–5418, https://doi.org/10.4049/jimmunol.1100225.
[74] L. Balas, P. Risé, D. Gandrath, G. Rovati, C. Bolego, F. Stellari, A. Trenti, C. Buccellati, T. Durand, A. Sala, Rapid metabolization of protectin D1 by β-oxidation of its polar head chain, J. Med. Chem. 62 (2019) 9961–9975, https://doi.org/10.1021/acs.jmedchem.9b01463.
[75] S. Bang, Y.-K. Xie, Z.-J. Zhang, Z. Wang, Z.-Z. Xu, R.-R. Ji, GPR37 regulates macrophage phagocytosis and resolution of inflammatory pain, J. Clin. Invest. 128 (2018) 3568–3582, https://doi.org/10.1172/JCI99888.
[76] H. Arnardottir, S. Thul, S.-C. Pawelzik, G. Karadimou, G. Artiach, A.L. Gallina, V. Mysdotter, M. Carracedo, L. Tarnawski, A.S. Caravaca, et al., The resolvin D1 receptor GPR32 transduces inflammation resolution and atheroprotection, J. Clin. Invest. 131 (2021), e142883, https://doi.org/10.1172/JCI142883.
[77] S. Krishnamoorthy, A. Recchiuti, N. Chiang, S. Yacoubian, C.-H. Lee, R. Yang, N. A. Petasis, C.N. Serhan, Resolvin D1 binds human phagocytes with evidence for proresolving receptors, Proc. Natl. Acad. Sci. U. S. A. 107 (2010) 1660–1665, https://doi.org/10.1073/pnas.0907342107.
[78] Y. Zhuang, L. Wang, J. Guo, D. Sun, Y. Wang, W. Liu, H.E. Xu, C. Zhang, Molecular recognition of formylpeptides and diverse agonists by the formylpeptide receptors FPR1 and FPR2, Nat. Commun. 13 (2022) 1054, https://doi.org/10.1038/s41467-022-28586-0.